Reaction of Silicon Ion (^2P) with Silane (SiH_4, SiD_4). Heats of Formation of SiH_n, SiH_n^+ (n = 1, 2, 3), and $Si_2H_n^+$ (n = 0, 1, 2, 3). Remarkable Isotope Exchange Reaction Involving Four Hydrogen Shifts

Bong Hyun Boo and P. B. Armentrout*†

Contribution from the Department of Chemistry, University of California, Berkeley, California 94720. *Received October 15, 1986*

Abstract: The reaction of ground-state silicon ion with silane is investigated by using a guided ion beam tandem mass spectrometer. Reaction cross sections of all possible fragments, $Si_mH_n^+$ (m = 1, 2; n = 0, 1, 2, 3), as a function of relative kinetic energy are determined. At thermal energies, the major product is $Si_2H_2^+$. One remarkable reaction, the interchange of the projectile silicon ion with the target silicon atom, is observed at near zero kinetic energy. Labeling experiments employing $^{30}Si^+$ for the beam or SiD_4 for the reactant indicate the intermediacy of the disilicon hydrides for the formation of the observed products. From the endothermicities of several reactions, the 298 K heats of formation for several ionic and neutral silicon hydrides are derived: $\Delta H_f°(SiH)$ = 90.0 ± 1.7, $\Delta H_f°(SiH_2)$ = 69.0 ± 2, $\Delta H_f°(SiH_3)$ = 48.5 ± 1.6, $\Delta H_f°(SiH_2^+)$ = 276.1 ± 1.7, $\Delta H_f°(SiH_3^+)$ = 237.1 ± 2, $\Delta H_f°(Si_2^+) \leq$ 328.0 ± 2, $\Delta H_f°(Si_2H^+) \leq$ 304.4 ± 1.6, $\Delta H_f°(Si_2H_2^+) \leq$ 268.0 ± 2.6, $\Delta H_f°(Si_2H_3^+)$ = 266 ± 2, all in kcal/mol. From an evaluation of these and other experiments, values of $\Delta H_f°(SiH_2^+)$ and $\Delta H_f°(SiH_2)$ of 278.0 ± 1.4 and 68.5 ± 1.5 kcal/mol, respectively, are recommended.

Reactive silicon hydrides have recently drawn considerable attention due to the interest in the chemical vapor deposition (CVD) of silicon in the electronics industry. In addition, the ion chemistry of these species is important for detailed modeling of plasma etching of silicon surfaces. However, the determination of reliable and systematic thermochemical properties for these short-lived radical and ionic species has been elusive and somewhat controversial. Recent experimental[1-6] and theoretical[7-9] work has begun to isolate consistent thermochemical data for these reactive silicon species, but uncertainties and ambiguities still exist.

In a recent study,[1] we examined the reaction of atomic silicon ions with molecular hydrogen, process 1, by using a guided ion beam mass spectrometer. We found that the bond energy derived

$$Si^+ + H_2 \rightarrow SiH^+ + H \quad (1)$$

from an analysis of the threshold for this reaction was in excellent agreement with spectroscopic data.[6] In the present study, we turn this experimental technique to the reaction of atomic silicon ions with silane. This system has been studied before at thermal energies[10] where the only product observed is $Si_2H_2^+$ and at 1 eV where $Si_2H_3^+$ was also observed.[11] However, we find that at higher kinetic energies a wide variety of silicon–hydride and disilicon–hydride ions and neutrals are formed. The mechanisms for these processes are discussed, and the energy dependences of the cross sections for individual product channels are interpreted to yield thermochemical data for both ionic and neutral species. This provides a completely different experimental approach to the determination of the thermochemical properties of silicon hydride neutrals and ions. The comparison of these values to others in the literature is discussed in some detail.

Experimental Section

Details of the guided ion beam apparatus are reported elsewhere.[12] Silicon ions are produced as described below. The ions are mass analyzed, decelerated to the desired translational energy, and injected into a radio frequency octopole ion beam guide which passes through the reaction chamber containing the silane reactant gas. The pressure of silane is kept low enough, $<8 \times 10^{-5}$ torr, that reaction products are the result of single collisions. The product and unreacted ions drift out of the gas chamber to the end of the guide where they are focused into a quadrupole mass filter and detected by a scintillation ion detector and standard ion pulse-counting techniques. The octopole beam guide creates a potential well which traps ions in the radial direction without affecting their axial energy. This greatly enhances the collection efficiency for the products and allows even small product channels to be detected.

Laboratory ion energies are converted to energies in the center of mass (CM) frame by using the conversion $E(CM) = E(lab) \times M/(m + M)$ where m and M are the masses of the projectile ion and target gas, respectively. The absolute zero of the energy scale is determined by using the octopole as a retarding energy analyzer. This procedure is detailed elsewhere.[12] We estimate that the uncertainty in the ion energy scale is ±0.05 eV lab (±0.03 eV CM).

Total reaction cross sections, σ_T, are calculated by using eq 2 where Q is the effective length of the interaction region (8.6 cm), n is the number density of the target gas, and I_R and I_P refer to the measured

$$I_R = (I_R + \sum I_P) \exp(-n\sigma_T Q) \quad (2)$$

intensities of transmitted reactant ions and product ions, respectively. Cross sections for the individual product channels are given by eq 3. We estimate that the absolute uncertainties in this study are approximately ±50%. Relative uncertainties are less than ≈5%.

$$\sigma_P = \sigma_T(I_P/\sum I_P) \quad (3)$$

Silicon ions are produced by either surface ionization (SI) or electron impact ionization followed by passage through a drift cell (EI/DC). In the SI source, a resistively heated rhenium filament at ≈2200 K is exposed to silane. Decomposition and ionization follow such that atomic silicon ions but no molecular ions are produced. Because the first excited state of Si^+ is 5.46 eV higher in energy than the ground state,[13] the SI source produces exclusively ground state $Si^+(^2P)$. The spread in the ion beam energy has a fwhm of 0.7 eV in the lab frame (0.4 eV CM). To reduce this distribution, silicon ions are also produced in the EI/DC source. Here the ions are formed by electron impact (EI) on silane in an ionization chamber. Since this can produce excited states of silicon

†NSF Presidential Young Investigator 1984–1989; Alfred P. Sloan Fellow.

(1) Elkind, J. L.; Armentrout, P. B. *J. Phys. Chem.* **1984**, *88*, 5454.
(2) Ding, A.; Cassidy, R. A.; Cordis, L. S.; Lampe, F. W. *J. Chem. Phys.* **1985**, *83*, 3426. Note that these authors use the stationary electron convention and $\Delta H_f°(SiH_4)$ = 7.3 kcal/mol. The values cited here have been corrected for these differences.
(3) Börlin, K.; Heinis, T.; Jungen, M. *Chem. Phys.* **1986**, *103*, 93. These authors use the stationary electron convention.
(4) Jasinski, J. M. *J. Phys. Chem.* **1986**, *90*, 555.
(5) Shin, S. K.; Beauchamp, J. L. *J. Phys. Chem.* **1986**, *90*, 1507.
(6) (a) Carlson, T. A.; Copley, J.; Duric, N.; Elander, N.; Erman, P.; Larsson, M.; Lyyra, M. *Astron. Astrophys.* **1980**, *83*, 238. (b) Douglas, A. E.; Lutz, B. L. *Can. J. Phys.* **1970**, *48*, 247.
(7) Pople, J. A.; Luke, B. T.; Frisch, M. J.; Binkley, J. S. *J. Phys. Chem.* **1985**, *89*, 2198.
(8) Ho, P.; Coltrin, M. E.; Binkley, J. S.; Melius, C. F. *J. Phys. Chem.* **1985**, *89*, 4647.
(9) Ho, P.; Coltrin, M. E.; Binkley, J. S.; Melius, C. F. *J. Phys. Chem.* **1986**, *90*, 3399.
(10) Henis, J. M. S.; Stewart, G. W.; Tripodi, M. K.; Gaspar, P. P. *J. Chem. Phys.* **1972**, *57*, 389.
(11) Yu, T.-Y.; Cheng, T. M. H.; Kempter, V.; Lampe, F. W. *J. Phys. Chem.* **1972**, *76*, 3321.
(12) Ervin, K. M.; Armentrout, P. B. *J. Chem. Phys.* **1985**, *83*, 166.
(13) Moore, C. E. *Natl. Stand. Ref. Data Ser. (U.S., Natl. Bur. Stand.)* **1970**, *34*.

0002-7863/87/1509-3549$01.50/0

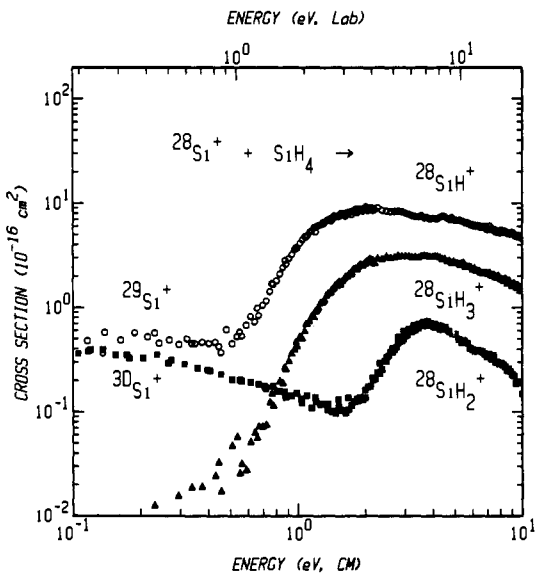

Figure 1. Variation of SiH_n^+ product cross sections with translational energy in the laboratory frame (upper scale) and the center of mass frame (lower scale) from the reaction of $^{28}Si^+$ with SiH_4. The low-energy components of the cross sections for mass 29 (open circles) and 30 (closed squares) correspond to the isotope exchange reactions, processes 7 and 15.

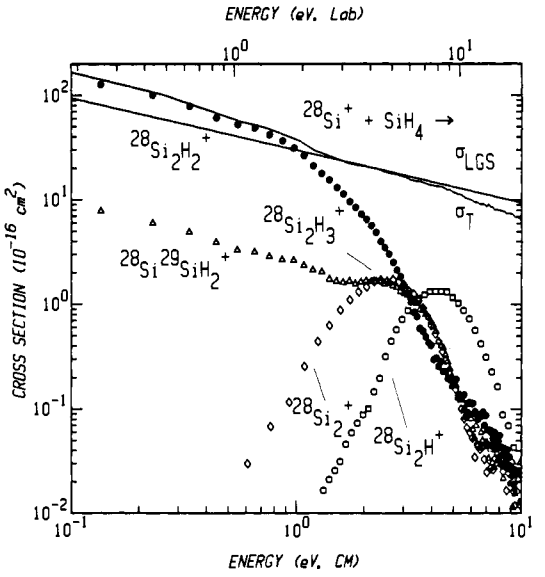

Figure 2. Variation of $Si_2H_n^+$ product cross sections with translational energy in the laboratory frame (upper scale) and the center of mass frame (lower scale) from the reaction of $^{28}Si^+$ with SiH_4. The lines show the cross section predicted by eq 10 (σ_{LGS}) and the total reaction cross section for all products in Figures 1 and 2. The low-energy component of the cross section for mass 59 (open triangles) corresponds to the contribution of $^{28}Si^{29}SiH_2^+$, process 35.

ions, the ions are injected into a high-pressure drift cell (DC) filled with Ar to pressures between 0.1 and 0.2 torr. Here, the ions are translationally and electronically thermalized by thousands of collisions with the inert gas. The resultant ion beam energy distribution has a fwhm of 0.3 eV lab (0.16 eV CM). One potential difficulty with this source is that very small amounts (<1%) of SiH^+ are produced and passed by the initial mass spectrometer. In some cases, this can produce some ambiguity in the cross section results for small channels. Such ambiguities are checked with the SI source which produces no SiH^+. Unless otherwise noted, the results presented here are obtained with the EI/DC source. Results obtained by using these two different sources are the same within experimental error save for the minor differences induced by the change in energy distribution.

Both the thermal motion of the reactant gas and the ion beam energy spread introduce an uncertainty in the collision energy. These energy distributions broaden any sharp features in the excitation functions, particularly endothermic thresholds. Both of these effects are taken into consideration when analyzing the results.[12]

The threshold regions of endothermic reactions are analyzed by using the empirical model, eq 4, where E_0 is the threshold energy, σ_0 is an energy-independent scaling factor, and n and m are variable parameters.

$$\sigma(E) = \sigma_0(E - E_0)^n/E^m \quad (4)$$

This general form has been discussed previously[14,15] and has been found to be quite useful in describing the shapes of endothermic reaction cross sections as well as for deriving accurate thermochemistry from the threshold energies. In the present study, we have chosen to restrict ourselves to forms of eq 4 where $m = 1$. This form has been predicted theoretically for translationally driven reactions.[16] In previous studies,[1,14,15] we have found that forms with $m = 1$ are often among the most useful in accurately describing the excitation functions.

At high energies, the observed reaction cross sections are generally observed to decline. This can be due either to dissociation of the product ion or to competition with other product channels. We have previously outlined a model for product dissociation which makes a simple statistical assumption within the constraints of angular momentum conservation.[17] Cross sections at high energy are analyzed by using eq 5 (a modified form

$$\sigma(E) = \sigma_0[(E - E_0)^n/E^m][1 - P_D] \quad (5)$$

of eq 4) where P_D is the probability of dissociation of the product ion.

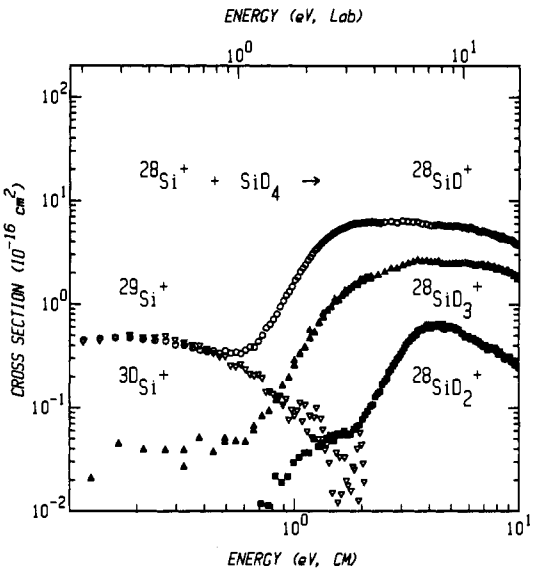

Figure 3. Variation of SiD_n^+ product cross sections with translational energy in the laboratory frame (upper scale) and the center of mass frame (lower scale) from the reaction of $^{28}Si^+$ with SiD_4. The low-energy component of the cross section for mass 30 (open circles) corresponds to the isotope-exchange reaction, process 12. Production of $^{29}Si^+$ in process 8 is shown by open triangles.

This probability is controlled by two parameters: p, which is related to the number of internal modes in the transition state, and E_D, which is the energy at which dissociation can begin (for $E < E_D$, $P_D = 0$). In this work, p and E_D are treated as variable parameters. E_D can then be related either to the bond energy of the ionic product or to the observed threshold for another reaction channel.[17]

Silane with semiconductor purity was purchased from Matheson Co. Deuteriated silane (SiD_4) was synthesized by the reduction of $SiCl_4$ with $LiAlD_4$ (98% purity).[18]

Results

Variation of the product cross sections with translational energy for reaction of Si^+ and SiH_4 is shown in Figures 1 and 2. To

(14) Ervin, K. M.; Armentrout, P. B. *J. Chem. Phys.* **1986**, *84*, 6738.
(15) Aristov, N.; Armentrout, P. B. *J. Am. Chem. Soc.* **1986**, *108*, 1806.
(16) Chesnavich, W. J.; Bowers, M. T. *J. Phys. Chem.* **1979**, *83*, 900.
(17) Weber, M. E.; Elkind, J. L.; Armentrout, P. B. *J. Chem. Phys.* **1986**, *84*, 1521. This paper gives E_D as $(D/f + E_0)$, where D is the ionic product dissociation energy and f is the average fraction of product internal energy in the ionic product.

(18) Gaspar, P. P.; Levy, C. A.; Adair, G. M. *Inorg. Chem.* **1970**, *9*, 1272.

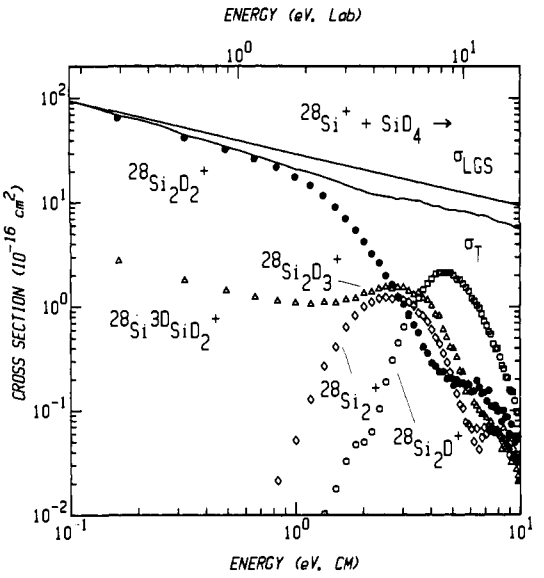

Figure 4. Variation of $Si_2D_n^+$ product cross sections with translational energy in the laboratory frame (upper scale) and the center of mass frame (lower scale) from the reaction of $^{28}Si^+$ with SiD_4. The lines show the cross section predicted by eq 10 (σ_{LGS}) and the total reaction cross section for all products in Figures 3 and 4. The low-energy component of the cross section for mass 62 (open triangles) corresponds to the contribution of $^{28}Si^{30}SiD_2^+$, process 37.

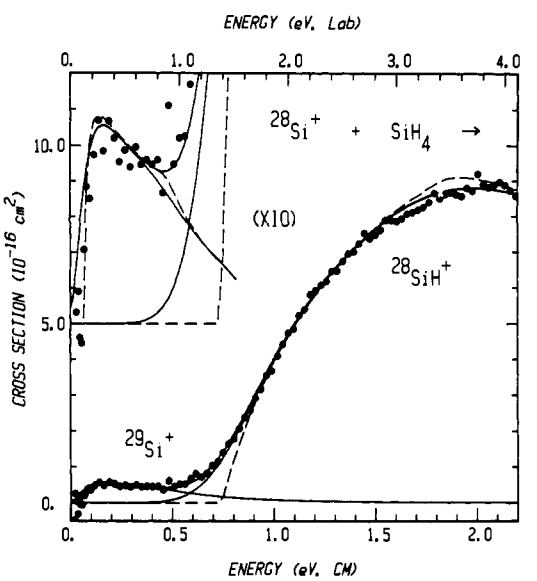

Figure 5. Cross section for mass 29 formed in reactions 6 and 7 as a function of the translational energy in the laboratory frame (upper scale) and the center of mass frame (lower scale). The experimental data (points) are compared with calculated cross sections for reactions 6 and 7 and their sum as described in the text and Table II. The full lines show the fits convoluted over the experimental energy distribution and the broken lines show the unconvoluted fits. The inset shows the cross sections expanded by a factor of 10 and offset from 0.

compare with the SiH_4 data, product cross sections for reaction with SiD_4 are shown in Figures 3 and 4. Comparison of these plots shows that chemically similar products generally have cross sections with similar magnitudes and shapes. Unambiguous identification of the products, however, relies on both thermochemical arguments and direct comparisons of the SiH_4 and SiD_4 systems. The details of these identifications follow.

Two difficulties are encountered in analyzing the cross sections for the individual products as a function of relative kinetic energy. One is the contribution of isotopic silicon and silicon hydrides to the other product channels. Silicon has three naturally occurring isotopes: ^{28}Si, 92.27% abundance; ^{29}Si, 4.68%; and ^{30}Si, 3.05%.[19] Therefore, it is possible to observe up to three silicon hydride species at one mass. Since the different species always have cross sections which vary differently with kinetic energy, we can usually identify the contributors based on their kinetic energy dependences. In all cases, unambiguous identification is provided by the kinetic energy dependences combined with employing $^{30}Si^+$ for the reactant ion beam or SiD_4 for the reactant neutral. The second difficulty faced is the overlap of one mass with adjacent masses. This occurs because mass resolution must sometimes be sacrificed in order to transmit ions efficiently through the quadrupole mass filter used for product analysis. This effect is a problem only for masses near the very large product ion, $Si_2H_2^+$. Experiments employing SiD_4 for the reactant provide well-resolved mass spectra for the individual products without a significant mass overlap effect. In all spectra shown below (except as noted), the results have been corrected for this mass overlap problem.

Mass 29: $^{28}Si^+ + SiH_4$. Figures 1 and 5 show the reaction cross section for mass 29 in reaction with silane. Two features are obvious, one at low energies and the major process beginning about 0.5 eV. Presumably, one of these features corresponds to reaction 6. This is certainly the lowest energy process for the

$$^{28}Si^+ + SiH_4 \rightarrow {}^{28}SiH^+ + SiH_3 \quad (6)$$

formation of $^{28}SiH^+$ in the $^{28}Si^+ + SiH_4$ system. Based on the available thermochemical data, Table I, the endothermicity of this reaction is given by the difference in the H_3Si-H and the Si^+-H bond energies, 0.64 ± 0.19 eV. Since this value is roughly consistent with the major process, the non-zero reactivity at low energy must be some other reaction. We believe this arises from process 7, a rather surprising reaction since it involves the transfer

$$^{28}Si^+ + {}^{29}SiH_4 \rightarrow {}^{29}Si^+ + {}^{28}SiH_4 \quad (7)$$

of all four hydrogens from one silicon center to another. If this isotopic silicon ion is truly being formed, we ought to be able to cleanly isolate process 7 by employing SiD_4 for the reactant, reaction 8. Figure 3 shows the reaction cross section observed

$$^{28}Si^+ + {}^{29}SiD_4 \rightarrow {}^{29}Si^+ + {}^{28}SiD_4 \quad (8)$$

for this process, and Figure 6 compares it directly with the cross section observed for reaction 7. It is apparent that these reactions

Table I. Heats of Formation (kcal/mol) at 298 K[a]

species	this work	literature: exptl	literature: theory
Si^+		297.1 (1)[b]	
SiH^+	273.5 (1.4)[c]	273.8 (1.2),[d] 274.2 (2.1)[e]	271.1[f]
SiH_2^+	276.1 (1.7)	264.5 (1.2),[g] 278.8 (0.9)[h] 279.2 (0.7),[i] 277.7 (0.6),[j] 277 (9)[k]	276.6[f]
SiH_3^+	237.1 (2)	239.5 (0.6),[h] ≤236.7 (1.2)[g] 236.6 (1.3),[i] ≤237.8,[j] 239 (9)[k]	233.0[f]
Si_2^+	≤328.0 (2)	313 (8)[l]	
Si_2H^+	≤304.4 (1.6)	315 (46)[k]	
$Si_2H_2^+$	≤268.0 (2.6)	286 (9)[k]	
$Si_2H_3^+$	266 (2)	245 (23)[k]	
Si		107.7 (1)[b]	
SiH	90.0 (1.7)	≥88.1,[m] 90,[n] 90.0 (2)[b] 85.1 (5.8),[q] 81.7 (1.2)[r]	91.7,[o] 88.3[p]
SiH_2	69.0 (2)	58,[n] 65.3 (1.5),[s] 69 (3)[t] 68.2 (0.8) or 65.2 (0.7)[j]	68.1,[o] 63.4[p]
SiH_3	48.5 (1.6)	46.4 (1.2)[n]	47.8,[o] 47.3[p]
SiH_4		8.2 (0.5)[b]	6.3[p]
Si_2		141 (3)[b]	
Si_2H			144.2 (3)[u]
Si_2H_2			89.5 (3)[u]
Si_2H_3			105.8 (3)[u]

[a] Ion heats of formation are calculated by using the thermal electron convention. [b] Reference 32. [c] Reference 1. [d] Reference 6a. [e] Reference 6b. [f] Reference 43. [g] Reference 3. [h] Reference 2. [i] Reference 37. [j] Reference 38. [k] Reference 49. [l] Reference 47. [m] Reference 31. [n] Reference 39. [o] Reference 8. [p] Reference 7. [q] Reference 30. [r] Reference 35. [s] Reference 40. [t] Reference 5. [u] Reference 9.

(19) Williams, D.; Yuster, P. *Phys. Rev.* **1946**, *69*, 556.

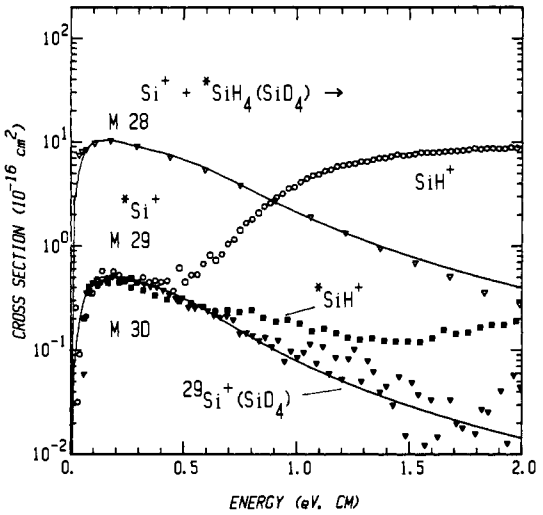

Figure 6. Apparent cross sections for the silicon isotope-exchange reactions 7 (open circles, reaction 6 at higher energies), 8 (solid triangles), 9 (open triangles), and 15 (solid squares, reactions 16 and 17 at higher energies) as a function of the translational energy in the laboratory frame (upper scale) and the center of mass frame (lower scale). The experimental data are compared to the convoluted fit (full lines) described in the text and Table II. An average threshold energy for reactions 8 and 9 is used in this calculation.

have similar energy dependences and cross section magnitudes at the lowest energies. Further evidence for process 7 is shown by the reaction of $^{30}Si^+$ (produced by SI) with SiH_4 in process 9, also shown in Figure 6. The cross section observed for reaction

$$^{30}Si^+ + {}^{28}SiH_4 \rightarrow {}^{28}Si^+ + {}^{30}SiH_4 \quad (9)$$

9 is 20 times larger than those for reactions 7 and 8 in the low energy range (<0.4 eV). This ratio correctly reflects the 19.7 ratio of the natural abundances of ^{28}Si (92.27%) and ^{29}Si (4.68%). Thus, the total cross section for the exchange of the projectile and target silicon atoms is 1.08 times larger than that shown for reaction 9, ≈11.1 Å^2 at low energy.

Analysis of the low-energy components of the cross sections for reactions 7–9 is accomplished by using eq 4. In every case, the excitation function with $n = 0.5$ and $m = 1.0$ gives a reasonable fit to the reaction cross sections, shown in Figures 5 and 6, when the threshold energy (E_0) lies in the range 0.07 ± 0.04 eV. The measured endothermicities and fitting parameters for this and other reactions examined below are summarized in Table II. This form for the cross section ($n = 0.5$, $m = 1$) can be derived by using microscopic reversibility arguments[20] from the common Langevin–Gioumousis–Stevenson (LGS) form[21] for exothermic ion-induced dipole interactions, eq 10, where e is the electron charge

$$\sigma(E) = \pi e(2\alpha/E)^{1/2} \quad (10)$$

and α is the polarizability of the neutral reactant. Since there is no significant difference (<1 meV) in the zero-point energies of the silanes having different silicon isotopes, reactions 7–9 are near thermoneutral. Thus, the rise of the cross sections at near zero kinetic energy indicates an effective barrier of 1.6 ± 1 kcal/mol for the exchange of the silicon atoms.

Above about 0.5 eV, the cross sections for processes 7–9 begin to fall off more sharply, Figure 6. This behavior is analyzed by using eq 5 with the values of p and E_D listed in Table II. This table also summarizes these values for other reactions studied below. Obviously, dissociation of the atomic product ion cannot account for this decrease. Therefore, it must be due to competition with other reaction channels. Indeed, the decline seems to correspond reasonably well with the onset of reaction 6, Figure 5. This suggests that reactions 6 and 7 share a common intermediate.

Since the cross section for reaction 7 is now well characterized, the cross section for reaction 6 can be obtained by subtracting the cross section for the $^{29}Si^+$ product channel from the total cross section for mass 29. Acceptable fits to this isolated cross section can be found with $n = 1.0 \pm 0.1$ and $m = 1.0 \pm 0.1$ in eq 4. The values center on the simple LOC form ($n = m = 1$) which gives a best fit when $E_0 = 0.74 \pm 0.05$ eV. This best fit and the sum of this fit and that for reaction 7 are shown in Figure 5. At high energies, the cross section for reaction 6 falls off slowly beginning about 1.8 eV. This seems primarily correlated with the decline in the total cross section, Figure 2. Some dissociation may occur at higher energies, but the threshold for decomposition to Si^+ + H cannot occur until ≈4 eV = $D°(H_3Si–H)$.

Table II. Values of n, E_0, p, and E_D Used to Model Cross Sections

system	product	n	E_0, eV[a]	p	E_D, eV
$Si^+ + {}^*SiH_4$	$^*Si^+$	0.5	0.07 (0.04)	1	0.46
	SiH^+	1.0	0.74 (0.05)	0	1.82
	SiH_2^+	1.6	1.72 (0.05)	1	3.68
	SiH_3^+	1.0	0.91 (0.05)	0	2.48
	Si_2^+	1.5	1.01 (0.05)	3	2.68
	Si_2H^+	1.5	2.26 (0.04)	3	4.19
	$Si_2H_2^+$	0.45	<0		
	$Si_2H_3^+$	1.5	0.57 (0.07)	3	2.47
$Si^+ + {}^*SiD_4$	$^*Si^+$	0.5	0.08 (0.04)	1	0.46
	SiD^+	1.0	0.76 (0.05)	0	2.12
	$^*SiD^+$	1.0	0.77 (0.04)	1	1.54
	SiD_2^+	1.6	1.85 (0.05)	1	3.87
	SiD_3^+	1.0	1.00 (0.06)	0	3.30
	Si_2^+	1.5	1.02 (0.06)	3	2.69
	Si_2D^+	1.5	2.29 (0.04)	3	4.70
	$Si_2D_2^+$	0.45	<0		
	$Si_2D_3^+$	1.5	0.61 (0.04)	2	2.80
$SiH^+ + SiH_4$	SiH_3^+	1.0	0.99 (0.04)	1	3.48
	Si_2H^+	1.3	0.97 (0.05)	2	2.85
	$Si_2H_2^+$	1.0	1.65 (0.1)	3	4.55
$Si^+ + CH_4$	CH_3^+	1.0	3.22 (0.04)	1	4.45
$Si^+ + CH_4$	SiH^+	1.0	1.27 (0.04)	0	4.56
$Si^+ + C_2H_6$	SiH_2^+	1.0	0.43 (0.04)	1	1.47
$Si^+ + C_2H_4$	SiH_2^+	1.5	0.85 (0.04)	3	2.18
$Si^+ + C_2D_6$	SiD_2^+	1.0	0.66 (0.04)	2	2.15
$Si^+ + C_3H_8$	SiH_2^+	1.8	0.44 (0.04)	2	2.25

[a] Uncertainties in parentheses.

Mass 30: $^{28}Si^+ + SiD_4$. In reaction with SiD_4, the analogue of reaction 6 is process 11. Also observed at this mass is a feature at low energy consistent with process 12, Figure 3. The cross

$$^{28}Si^+ + SiD_4 \rightarrow {}^{28}SiD^+ + SiD_3 \quad (11)$$

$$^{28}Si^+ + {}^{30}SiD_4 \rightarrow {}^{30}Si^+ + {}^{28}SiD_4 \quad (12)$$

section behavior and magnitude in this region are in accord with those for reaction 7 after correcting for the isotopic abundances of $^{30}Si^+$ and $^{29}Si^+$. Analysis of reaction 11 (after correcting for the presence of process 12) shows that the LOC form gives the best fit as found above for reaction 6. The endothermicity of process 11 is found to be 0.76 ± 0.05 eV. The high energy behavior of reaction 11 is similar to that for reaction 6.

Mass 31: $^{28}Si^+ + SiD_4$. Figure 7 shows the cross section for mass 31 formed in reaction with SiD_4. This must correspond to reaction 13 and should have the same threshold as reaction 11, 0.76 ± 0.05 eV. Analysis of this cross section with the LOC form

$$^{28}Si^+ + {}^{29}SiD_4 \rightarrow {}^{29}SiD^+ + {}^{28}SiD_3 \quad (13)$$

yields a threshold of 0.77 ± 0.05 eV, in excellent agreement with the expected value. It is interesting to note that the magnitude of this cross section at ≈1 eV is over 100 times smaller than for reaction 11 (which has a comparable cross section magnitude to reaction 6). Even after correcting for the isotopic abundances (a factor of 19.7), the cross section is ≈5 times smaller than that for reaction 11. As discussed below, a careful account of the isotopic exchange reaction explains this observation.

At intermediate energies, the cross section falls off much more sharply than for reaction 11. This occurs at an energy well below any dissociation process and therefore is due to competition with other reaction channels. At still higher energies, the cross section shows a second feature. This is probably due to reaction 14, a

(20) Levine, R. D.; Bernstein, R. B. *J. Chem. Phys.* **1972**, *56*, 2281.
(21) Gioumousis, G.; Stevenson, D. P. *J. Chem. Phys.* **1958**, *29*, 294.

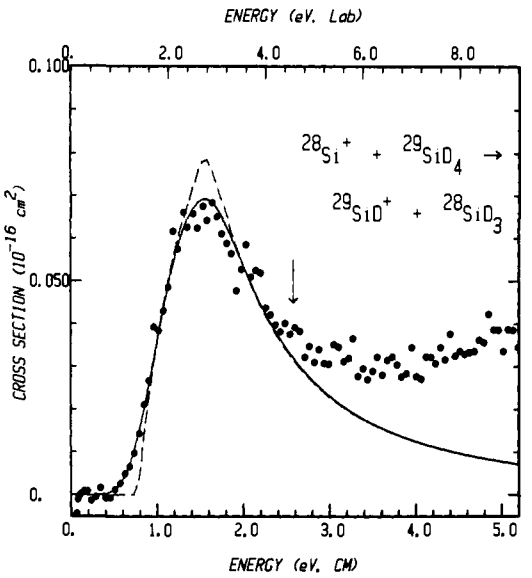

Figure 7. Cross section for mass 31 formed in reactions 13 and 14 as a function of the translational energy in the laboratory frame (upper scale) and the center of mass frame (lower scale). The experimental data (points) are compared with the calculated cross section for reaction 13 as described in the text and Table II. The full line shows the fit convoluted over the experimental energy distribution, and the broken line shows the unconvoluted fit. The arrow at 2.60 eV indicates the thermodynamic onset of reaction 14.

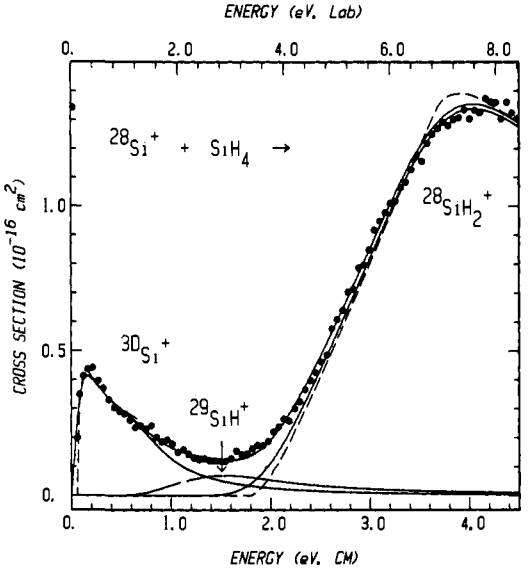

Figure 8. Cross section for mass 30 formed in reactions 15, 16, and 17 as a function of the translational energy in the laboratory frame (upper scale) and the center of mass frame (lower scale). The experimental data (points) are compared with calculated cross sections for reactions 15, 16, and 17 and their sum as described in the text and Table II. The full lines show the fits convoluted over the experimental energy distribution, and the broken lines show the unconvoluted fits.

process which is expected to have a threshold of 2.6 ± 0.1 eV, Table I. This is consistent with the data, Figure 7.

$$^{28}Si^+ + {}^{29}SiD_4 \rightarrow {}^{29}SiD^+ + {}^{28}SiD + D_2 \quad (14)$$

Mass 30: $^{28}Si^+ + SiH_4$. Figures 1 and 8 show the reaction cross section for mass 30. Possible structures for this mass are $^{30}Si^+$, $^{29}SiH^+$, and $^{28}SiH_2^+$, which correspond to reactions 15, 16, and 17, respectively. The cross section at near zero kinetic energy

$$^{28}Si^+ + SiH_4 \rightarrow {}^{30}Si^+ + {}^{28}SiH_4 \quad (15)$$

$$^{28}Si^+ + SiH_4 \rightarrow {}^{29}SiH^+ + {}^{28}SiH_3 \quad (16)$$

$$^{28}Si^+ + SiH_4 \rightarrow {}^{28}SiH_2^+ + SiH_2 \quad (17)$$

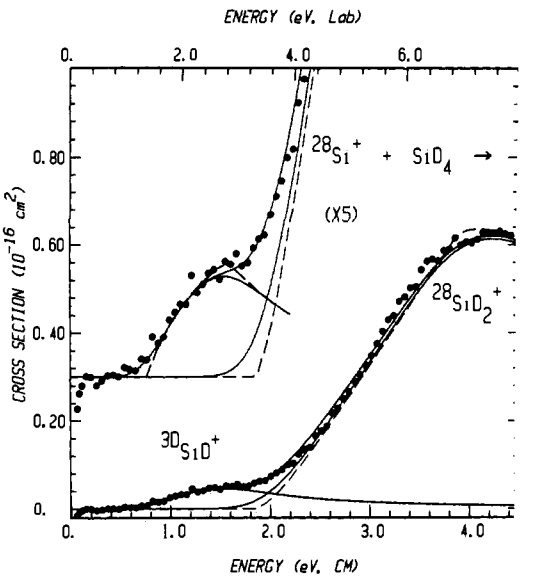

Figure 9. Cross section for mass 32 formed in reactions 18 and 19 as a function of the translational energy in the laboratory frame (upper scale) and the center of mass frame (lower scale). The experimental data (points) are compared with calculated cross sections for reactions 18 and 19 and their sum as described in the text and Table II. The full lines show the fits convoluted over the experimental energy distribution, and the broken lines show the unconvoluted fits. The inset shows the cross sections expanded by a factor of 5 and offset from 0.

is due to reaction 15. As shown in Figure 6, it has the same energy dependence as reactions 7, 8, and 9 and also the proper magnitude given by the isotopic abundances, 0.65 times less than reaction 7. The difference between the shape of this cross section and that for reaction 7 in the range 0.4–1.6 eV reflects the appearance of reaction 16. This should have the same energy dependence as reaction 13 and a similar magnitude. The true cross section for the SiH_2^+ product can be obtained by subtraction of the cross sections contributed by reactions 15 and 16. Figure 8 shows that the sum of these three cross section components accurately reproduces the data. The veracity of this extensive modeling is verified in the SiD_4 system (next section). At high energies, the cross section for reaction 17 declines beginning at ≈4 eV. This probably corresponds to dissociation to $SiH^+ + H$, which can begin at ≈3.8 eV, Table I.

Mass 32: $^{28}Si^+ + SiD_4$. Figures 3 and 9 show the production of mass 32 from SiD_4. The feature in the low-energy region of Figure 8 is completely gone, as expected. Instead we observe a small rise in the cross section in the intermediate energy range, $0.6 < E < 2.0$ (eV). The threshold behavior of the low-energy cross section is quite similar to that for the cross section for $^{29}SiD^+$ formed in reaction 13. The fact that the magnitude is also comparable strongly suggests that the feature arises from reaction 18.

$$^{28}Si^+ + {}^{30}SiD_4 \rightarrow {}^{30}SiD^+ + SiD_3 \quad (18)$$

Subtraction of the cross section for $^{30}SiD^+$ from the total cross section gives the isolated cross section for $^{28}SiD_2^+$ formed in reaction 19. Analysis of this is straightforward and uses the same

$$^{28}Si^+ + SiD_4 \rightarrow {}^{28}SiD_2^+ + SiD_2 \quad (19)$$

excitation function as for reaction 17. The sum of these two cross section components reproduces the data nicely, Figure 9. The high energy behavior is similar to reaction 17.

Mass 31: $^{28}Si^+ + SiH_4$. Figures 1 and 10 show the experimental results for mass 31. Possible structures are $^{30}SiH^+$, $^{29}SiH_2^+$, and $^{28}SiH_3^+$ due to reactions 20, 21, and 22, respectively. The

$$^{28}Si^+ + SiH_4 \rightarrow {}^{30}SiH^+ + {}^{28}SiH_3 \quad (20)$$

$$^{28}Si^+ + SiH_4 \rightarrow {}^{29}SiH_2^+ + {}^{28}SiH_2 \quad (21)$$

$$^{28}Si^+ + SiH_4 \rightarrow {}^{28}SiH_3^+ + SiH \quad (22)$$

major product channel for this mass is most likely the hydride

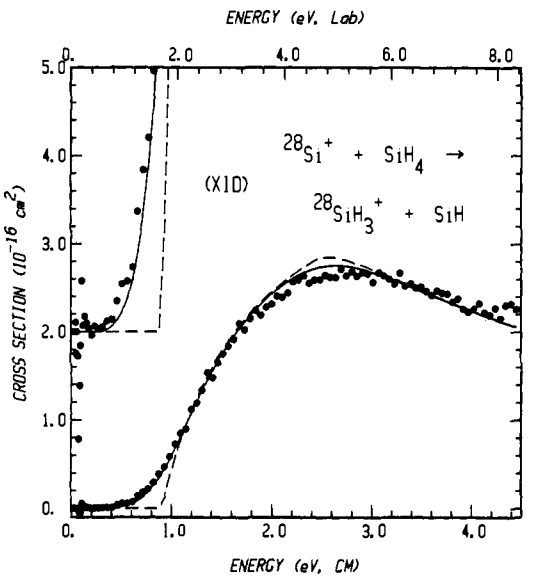

Figure 10. Cross section for mass 31 formed primarily in reaction 22 as a function of the translational energy in the laboratory frame (upper scale) and the center of mass frame (lower scale). The experimental data (points) are compared with the calculated cross section for reaction 22 as described in the text and Table II. The full line shows the fit convoluted over the experimental energy distribution, and the broken line shows the unconvoluted fit. The inset shows the cross sections expanded by a factor of 10 and offset from 0.

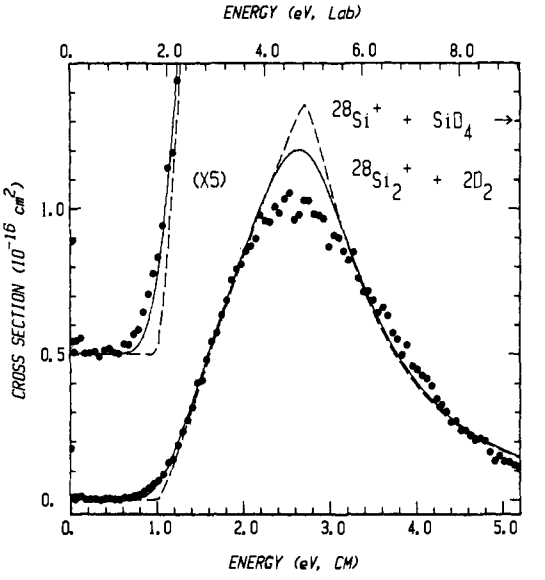

Figure 11. Cross section for mass 56 formed in reaction 26 as a function of the translational energy in the laboratory frame (upper scale) and the center of mass frame (lower scale). The experimental data (points) are compared with the calculated cross section for reaction 26 as described in the text and Table II. The full line shows the fit convoluted over the experimental energy distribution, and the broken line shows the unconvoluted fit. The inset shows the cross sections expanded by a factor of 5 and offset from 0.

transfer reaction, process 22. Contributions of reactions 20 and 21 to the total cross sections for mass 31 are deduced to be less than 4% based on the results for reactions 6 and 17. Neglecting these small contributions, we analyze the cross section for reaction 22 as given in Table II. The result is shown in Figure 10.

The cross section for process 22 levels out beginning about 2 eV. This may correlate with the onset of reaction 17 but may also correspond to dissociation to $SiH^+ + H_2$ beginning about 2.5 eV. At energies above 4–5 eV, the cross section begins to decline more rapidly. This may indicate the onset of dissociation to $SiH_2^+ + H$, which has a thermodynamic threshold of ≈5.0 eV.

Mass 34: $^{28}Si^+ + SiD_4$. The two possible structures for mass 34, Figure 3, are $^{30}SiD_2^+$ and $^{28}SiD_3^+$, which should arise from reactions 23 and 24, respectively. The contribution from reaction

$$^{28}Si^+ + SiD_4 \rightarrow {}^{30}SiD_2^+ + {}^{28}SiD_2 \quad (23)$$

$$^{28}Si^+ + SiD_4 \rightarrow {}^{28}SiD_3^+ + SiD \quad (24)$$

23 to the total cross section for mass 34 is deduced to be negligibly small. The endothermicity of reaction 24 is derived directly from analysis of the total cross section for mass 34. As for reaction 22, the LOC form gives the best fit, Table II. The high-energy behavior is similar to reaction 22.

Mass 56: $^{28}Si^+ + SiH_4$, $^{28}Si^+ + SiD_4$. Figures 2 and 4 indicate the reaction cross sections for mass 56 formed in reactions with SiH_4 and SiD_4, respectively. The cross sections at energies near threshold in reaction with SiD_4 are shown in Figure 11. $^{28}Si_2^+$ is the only possible ion at this mass for both systems. At low energies, it must be formed in processes 25 and 26. Based on

$$^{28}Si^+ + {}^{28}SiH_4 \rightarrow {}^{28}Si_2^+ + 2H_2 \quad (25)$$

$$^{28}Si^+ + {}^{28}SiD_4 \rightarrow {}^{28}Si_2^+ + 2D_2 \quad (26)$$

the literature thermochemistry, Table I, the expected threshold for reaction 25 is 0.33 ± 0.35 eV and for reaction 26 is 0.40 ± 0.35 eV. The apparent threshold of the data for both systems is higher than this, E_0 = 1.01 ± 0.05 eV for reaction 25 and 1.02 ± 0.06 eV for reaction 26. The fit for the latter system is shown in Figure 11. It is possible that the true threshold is not observed in these reactions due to competition with other less endothermic product channels.

At intermediate energies the cross section declines beginning at ≈2.7 eV. Since dissociation of Si_2^+ cannot occur until 4.3 eV, this is presumably due to competition from other channels, probably formation of Si_2H^+, Figures 2 and 4. A second feature in the $^{28}Si_2^+$ cross section can be seen in Figure 4 beginning about 6 eV. This same feature appears in Figure 2 but is much less obvious. This alternative pathway for production of Si_2^+ is presumably reaction 27. This process can begin about 5.5 eV, i.e., 4.5 eV ($=D°(D_2)$) above the endothermicity of reaction 26.

$$^{28}Si^+ + {}^{28}SiD_4 \rightarrow {}^{28}Si_2^+ + D_2 + 2D \quad (27)$$

Mass 57: $^{28}Si^+ + SiH_4$. Figure 2 shows the cross section for mass 57. Possible structures for mass 57 are $^{28}Si^{29}Si^+$ and $^{28}Si_2H^+$ from reactions 28 and 29, respectively. The cross section for

$$^{28}Si^+ + SiH_4 \rightarrow {}^{28}Si^{29}Si^+ + 2H_2 \quad (28)$$

$$^{28}Si^+ + SiH_4 \rightarrow {}^{28}Si_2H^+ + H_2 + H \quad (29)$$

reaction 28 should look the same as that for reaction 25 but must be reduced in magnitude according to the different isotopic abundances of ^{28}Si and ^{29}Si, a factor of 19.7. While this contribution can explain the initial onset of mass 57, reaction 29 must be occurring at higher energies. After reaction 28 is accounted for, the cross section for process 29 can be reproduced with the excitation function given in Table II. The cross section declines above ≈5 eV. Dissociation to $SiH^+ + Si$ or $Si_2^+ + H$ can occur beginning about 5.5 eV and to $Si^+ + SiH$ at about 5.8 eV.

Mass 58: $^{28}Si^+ + SiD_4$. The cross section for mass 58 formed in reaction with SiD_4 is shown in Figure 4 and again in Figure 12. Reactions 30 and 31 account for this mass. The cross section

$$^{28}Si^+ + SiD_4 \rightarrow {}^{28}Si^{30}Si^+ + 2D_2 \quad (30)$$

$$^{28}Si^+ + SiD_4 \rightarrow {}^{28}Si_2D^+ + D_2 + D \quad (31)$$

for reaction 30 has the same shape as that for process 26 but is reduced by a factor of 30.3 (=92.27/3.05). After this contribution is subtracted, the same excitation function used to analyze reaction 29 is used here, Figure 12. The high-energy behavior of the cross section is similar to that for reaction 29.

Mass 58: $Si^+ + SiH_4$. Mass 60: $Si^+ + SiD_4$. Figures 2 and 4 show the cross sections for mass 58 and mass 60 in reactions with SiH_4 and SiD_4, respectively. These two masses must cor-

$$^{28}Si^+ + SiH_4 \rightarrow {}^{28}Si_2H_2^+ + H_2 \quad (32)$$

$$^{28}Si^+ + SiD_4 \rightarrow {}^{28}Si_2D_2^+ + D_2 \quad (33)$$

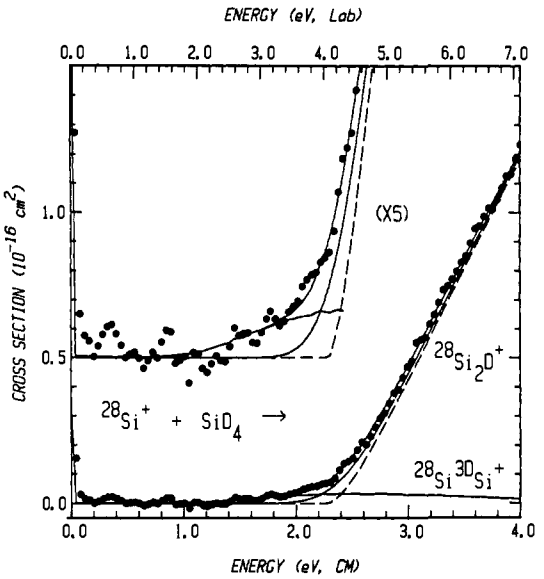

Figure 12. Cross section for mass 58 formed in reactions 30 and 31 as a function of the translational energy in the laboratory frame (upper scale) and the center of mass frame (lower scale). The experimental data (points) are compared with the cross section for reaction 26 (scaled by the isotope ratio of ^{28}Si and ^{30}Si), the calculated cross section for reaction 31 as described in the text and Table II, and their sum. The full lines show the fits convoluted over the experimental energy distribution, and the broken line shows the unconvoluted fit. The inset shows the cross sections expanded by a factor of 5 and offset from 0.

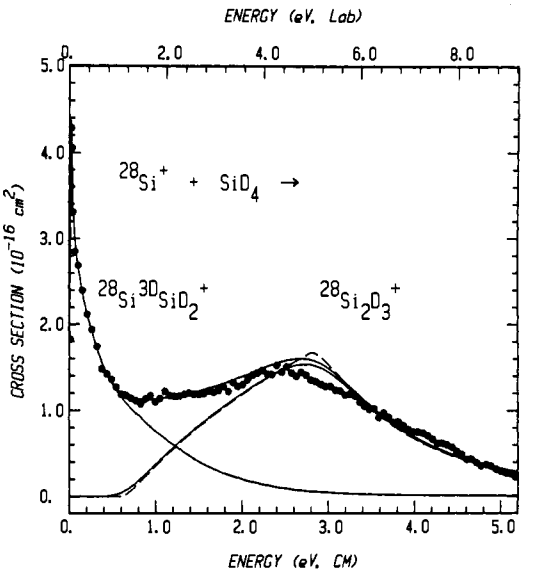

Figure 13. Cross section for mass 62 formed in reactions 37 and 38 as a function of the translational energy in the laboratory frame (upper scale) and the center of mass frame (lower scale). The experimental data (points) are compared with the cross section for reaction 33 (scaled to the observed cross section), the calculated cross section for reaction 38 as described in the text and Table II, and their sum. The full lines show the fits convoluted over the experimental energy distribution, and the broken line shows the unconvoluted fit.

respond to reactions 32 and 33. The energy dependences of the cross sections for these product channels are essentially the same. At energies less than 0.8 eV, the cross sections decline as $E^{-0.55}$, close to the prediction of the LGS model, eq 10. Beginning about 1 eV, the cross sections fall off as $E^{-2.0}$. Since the total cross sections do not decline in this fashion, Figures 2 and 4, this decrease must be due to decomposition of $Si_2H_2^+$ ($Si_2D_2^+$) in process 25 (26) or to depletion of a common reaction intermediate via processes 6 and 22 (11 and 24). This is consistent with the endothermicities 1.01, 0.74, and 0.91 eV of reactions 25, 6, and 22, respectively. Reaction 6 (11) is the main channel leading to this decrease since it is the only process with a cross section big enough to account for the decline in reaction 32 (33).

Above 2 eV the cross sections fall off sharply with an energy dependence of $E^{-4.9}$. This seems to correlate with the fragmentation of $Si_2H_2^+$ into Si_2H^+ and H, reaction 29 (31), beginning at 2.26 eV. At still higher energies (3–10 eV), the cross section for $Si_2H_2^+$ declines more slowly. This feature is more obvious in the cross section for $Si_2D_2^+$ at 4–7 eV, Figure 4. This must correspond to the onset of another channel for formation of $Si_2H_2^+$, process 34 (and its deuterium analogue). This will occur at 4.5 eV ($=D°(H_2)$) above the exothermicity of reaction 32 (33).

$$Si^+ + SiH_4 \rightarrow Si_2H_2^+ + 2H \quad (34)$$

Mass 59: $^{28}Si^+ + SiH_4$. The cross section for mass 59 in reaction with SiH_4 is shown in Figure 2. At low energies, this is due primarily to reaction 35, but at higher energies, reaction 36 also contributes. In fact, the exothermic component is 0.061

$$^{28}Si^+ + SiH_4 \rightarrow {}^{28}Si^{29}SiH_2^+ + H_2 \quad (35)$$

$$^{28}Si^+ + SiH_4 \rightarrow {}^{28}Si_2H_3^+ + H \quad (36)$$

times smaller than the cross section for reaction 32. Based on isotopic abundances, the calculated ratio should be 0.051. The additional amount is probably due to a slight mass overlap with mass 58, $^{28}Si_2H_2^+$. The true cross section of reaction 36 can be found by subtraction of the cross section from reaction 35 and the mass overlap, which have the same energy dependence. Analysis of the excitation function, Table II, provides an endothermicity for reaction 36 of 0.57 ± 0.07 eV. This value is in reasonable agreement with 0.3 eV recommended by Yu et al.[11] At energies above 2 eV, the cross section declines. This seems correlated with decomposition to $Si_2H^+ + H_2$, which has a threshold at 2.26 eV.

Mass 62: $^{28}Si^+ + SiD_4$. Figures 4 and 13 show the cross section for mass 62 in reaction with SiD_4. Processes 37 and 38 explain this species. At low energies, the ratio of mass 60 to mass 62 is

$$^{28}Si^+ + SiD_4 \rightarrow {}^{28}Si^{30}SiD_2^+ + D_2 \quad (37)$$

$$^{28}Si^+ + SiD_4 \rightarrow {}^{28}Si_2D_3^+ + D \quad (38)$$

0.039 compared to the expected isotopic ratio of 0.033. The subtracted cross section for reaction 38 is fit with the same excitation function as for reaction 36, Table II. At high energy, the cross section reaches a maximum between 2 and 3 eV, suggesting dissociation to $Si_2D^+ + D_2$ which begins at 2.29 eV.

Discussion

Reaction Efficiency. As shown in Figures 2 and 4, the energy dependence of the total cross sections for reaction of Si^+ with both SiH_4 and SiD_4 is roughly in accord with the LGS form, eq 10. The absolute magnitudes are also in fair agreement with this prediction when the polarizabilities of SiH_4 and SiD_4 are taken to be 3.1 ± 0.4 Å^3.[22] Clearly, $Si^+(^2P)$ reacts on nearly every collision with silane. This suggests that insertion of Si^+ into the Si–H bond is facile, consistent with the fact that Si^+ can insert into H_2.[1] This may be facilitated by the polarity of the Si–H bonds in silane (the silicon atom in silane has a charge of about +0.5).[23]

To compare the present results with those of previous studies, we convert our measured cross sections into rate constants for the exothermic channels, reactions 32 and 33. This is achieved by using eq 39 where $v = (2E/\mu)^{1/2}$, μ being the reduced mass of

$$k(\langle E \rangle) = v\sigma(E) \quad (39)$$

the reactants. $\langle E \rangle$ is the mean relative energy of the reactants and equals $E + {}^3/_2\gamma kT$, where $\gamma = m/(m + M)$ and T is the temperature of the reactant gas (here, 305 K). Below 0.8 eV, where the cross section decreases with an energy dependence of

(22) Polarizability of SiH_4, 3.1 ± 0.4 Å^3, is calculated by the semiempirical method of Miller and Savchick [Miller, K. J.; Savchick, J. A. *J. Am. Chem. Soc.* **1979**, *101*, 7206]. SiF_4 and $SiCl_4$ were used as reference compounds for these calculations. The polarizabilities for these species were taken from Rothe and Bernstein [Rothe, E. W.; Bernstein, R. B. *J. Chem. Phys.* **1959**, *31*, 6].

(23) Luke, B. T.; Pople, J. A.; Krogh-Jespersen. M.-B.; Apeloig, Y.; Chandrasekhar, J.; Schleyer, P. v. R. *J. Am. Chem. Soc.* **1986**, *108*, 260.

Scheme I

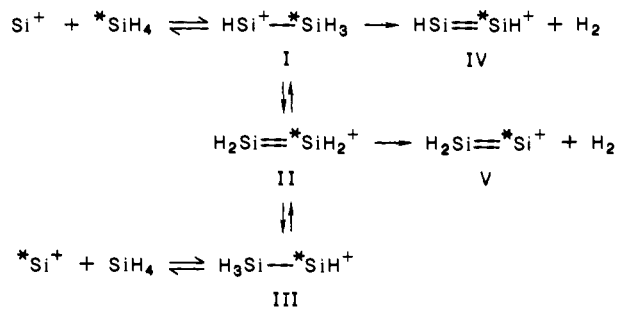

$E^{-0.55}$, the rate constant is nearly constant at $1.5 \pm 0.2 \times 10^{-9}$ cm^3/s for reaction 32. For the SiD_4 system, $k = 0.8 \pm 0.2 \times 10^{-9}$ cm^3/s. These experimental values are in good agreement with the LGS theoretical value of $1.1 \pm 0.1 \times 10^{-9}$ cm^3/s given by eq 40.[21,22]

$$k = 2\pi e(\alpha/\mu)^{1/2} \quad (40)$$

Ion cyclotron resonance (ICR) results of Henis et al.[10] provide a thermal rate constant for reaction 32 of $0.48 \pm 0.06 \times 10^{-9}$ cm^3/s. Tandem mass spectrometer results of Yu et al.[11] at 1 eV provide a value of $0.32 \pm 0.03 \times 10^{-9}$ cm^3/s. These values are in fair agreement with the present results.

Reaction Mechanism. The first step in the reaction of Si^+ with $*SiH_4$ is presumably insertion to form I, Scheme I. Ejection of $*Si^+$ in the isotope exchange reaction requires that I undergo hydrogen transfer yielding III. Decomposition of III can then occur by elimination of SiH_4, the microscopic reverse of the initial insertion step. The isomerization of I to III almost certainly involves the disilene ion II since concerted hydrogen atom transfer seems unlikely. The intermediacy of II is reasonable since it has been suggested that a neutral silylsilylene (the neutral analogue of I) rearranges to disilene by H migration with only a small energy barrier.[9,24,25] Recently, evidence for a similar interconversion of an α-silylsilylene, $HSiSiMe_3$, to an isomeric silylsilylene, $HMe_2SiSiMe$, via the disilene, $HMeSi{=}SiMe_2$, has also been presented.[26]

Dissociation of $Si_2H_4^+$ into $Si_2H_2^+$ and H_2 is the most efficient process at low energies, accounting for over 90% of the products. This product could arise from 1,1-dehydrogenation from I (or III) to form IV, a process stabilized by the formation of the Si–Si π bond. An alternative isomer V could be formed by 1,1-dehydrogenation of II. Alternate pathways involve 1,2-dehydrogenation of II to form IV or of I (or III) to form V. These four-center eliminations are probably less likely since they are symmetry forbidden and therefore should have relatively high energy barriers. At higher energies, $Si_2H_4^+$ can lose a hydrogen atom to form $Si_2H_3^+$. This in turn decomposes primarily by dehydrogenation to form Si_2H^+ but also by hydrogen atom loss to again yield $Si_2H_2^+$, reaction 34. At the lowest energies, Si_2^+ must be formed by dehydrogenation of $Si_2H_2^+$. The monosilicon hydride products, SiH^+ and SiH_3^+, can arise simply from Si–Si bond cleavage of I (or III). SiH_2^+ could arise from Si–Si bond cleavage of II or by elimination of SiH_2 from I or III. The relative efficiencies for the individual channels appear to correspond closely to the relative stabilities of the products.

It is interesting to examine the relative rate of the Si–Si bond cleavage of the primary intermediate I to the interconversion of I to III. This can be derived by comparing the cross sections for formation of SiH^+ (from I) and of $*SiH^+$ (from III). These are most easily seen for reactions 11 and 13 in the SiD_4 system. Correcting for the isotopic distributions, we find that these cross sections are given by eq 41 and 42. These calculated cross

$$\sigma(SiD^+) = \sigma(11) - \sigma(13)(92.27/4.68) \quad (41)$$

$$\sigma(*SiD^+) = \sigma(13)(100/4.68) \quad (42)$$

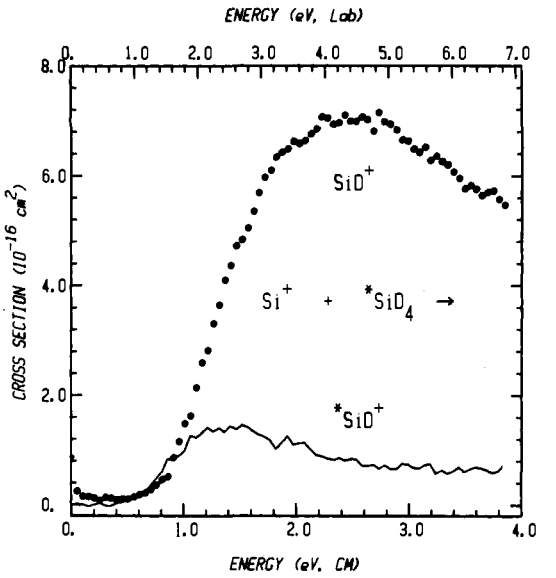

Figure 14. Cross sections for SiD^+, eq 41, and $*SiD^+$, eq 42, as a function of the translational energy in the laboratory frame (upper scale) and the center of mass frame (lower scale).

Scheme II

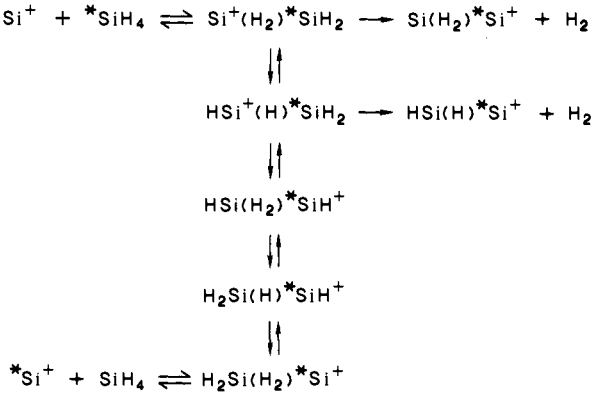

sections, Figure 14, show that until $\approx$1 eV the probability of forming $*SiD^+$ is the same as for SiD^+. This makes it clear that at low energies the isomerization between I and III is fast compared with the decomposition of I and III by Si–Si bond cleavage. At higher energies, much more SiD^+ is formed than $*SiD^+$, indicating that decomposition of I is now faster than isomerization to III.

While the hydrocarbon-like species in Scheme I would seem natural choices for the most stable forms of this ion, ab initio calculations on the neutral Si_2H_2 find that the most stable structure is a doubly bridged isomer, $Si(H_2)Si$.[27] Likewise in hydrocarbon ions, bridged species are apparently abundant. This makes it unclear whether structures I, II, and III are true minima (or even local minima) on the potential energy surface of the $Si^+ + SiH_4$ reaction. Indeed, we have performed a MNDO calculation[28] which indicates that the doubly bridged isomer, $Si(H_2)SiH_2^+$, may be the most stable $Si_2H_4^+$ species. This calculation also indicates that $HSi(H)SiH_2^+$ is a local minimum on the potential energy surface. Scheme II shows an alternate reaction mechanism for the isotope exchange and dehydrogenation processes which involves such bridged species. Ab initio calculations on these possible structures would be of obvious interest in this regard.

Thermochemistry. As noted above, the threshold behavior for the various product channels is analyzed by using eq 4 with m

(24) Krogh-Jesperson, K. *Chem. Phys. Lett.* **1982**, *93*, 327.
(25) Boo, B. H. Ph.D. Dissertation, Washington University in St. Louis, 1984.
(26) Boo, B. H.; Gaspar, P. P. *Organometallics* **1986**, *5*, 698.
(27) Binkley, J. S. *J. Am. Chem. Soc.* **1984**, *106*, 603. Lischka, H.; Köhler, H. J. *Ibid.* **1983**, *105*, 6646.
(28) Dewar, M. J. S.; Thiel, W. *J. Am. Chem. Soc.* **1977**, *99*, 4899. Dewar, M. J. S.; McKee, M. L.; Rzepa, H. S. *Ibid.* **1978**, *100*, 3607. Dewar, M. J. S.; Friedheim, J.; Grady, G.; Healy, E. F.; Stewart, J. J. P. *Organometallics* **1986**, *5*, 375.

Table III. Conversions between Protiated and Deuteriated Species and between 0 and 298 K Values in kcal/mol

species	ΔZPE^a	$\Delta\Delta H_f°^b$	$\Delta H_f°_{298} - \Delta H_f°_0$
SiH	0.82[c]	−0.1	0.4
SiH_2	1.92[d]	0.1	−0.4
SiH_3	3.58[e]	0.9	−1.3
SiH_4	5.23[f]	1.5	−2.3
SiH^+	0.86[g]	−0.1	1.8
SiH_2^+	1.99[h]	0.2	1.1
SiH_3^+	3.71[h]	1.0	0.2
H_2	1.84[i]		

[a] Difference in zero-point energies between $SiH_n^{(+)}$ and $SiD_n^{(+)}$, $ZPE[SiH_n^{(+)}] - ZPE[SiD_n^{(+)}]$. Values are calculated by using the vibrational frequencies obtained from the indicated references. Values for SiD_n are calculated from these if not available directly. [b] $\Delta H_f°[SiH_n^{(+)}] - \Delta H_f°[SiD_n^{(+)}]$. [c] Herzberg, G.; Lagerqvist, A.; Mckenzie, B. J. *Can. J. Phys.* **1969**, *47*, 1889. [d] Fredin, L.; Hauge, R. H.; Kafafi, Z. H.; Margrave, J. L. *J. Chem. Phys.* **1985**, *82*, 3542. [e] Allen, W. D.; Schaefer, H. F., unpublished results. [f] Shimanouchi, T. *Natl. Stand. Ref. Data Ser. (U.S., Natl. Bur. Std.)* **1972**, *39*. [g] Reference 6. [h] Reference 43. [i] Reference 32.

= 1. The results are summarized in Table II. It can be seen that values of n ranging from 1 (the simple line-of-centers model) to 1.6 allow the experimental cross sections at energies near threshold to be accurately reproduced. The uncertainties listed in Table II include those arising from the determination of the best value of n, the variation in different data sets (between three and five sets are evaluated for each product channel), and the absolute error in the energy scale, 0.03 eV. If it is assumed that there are no energy barriers in excess of the true endothermicity of the reaction, then these thresholds can be converted to thermochemical data for the products. This assumption is often quite reasonable for ion–molecule reactions since the long-range ion-induced dipole attraction eliminates small energy barriers.[29] Clearly, no activation barrier to the initial insertion step is observed, as discussed above. Our previous study of reaction 1 demonstrates the veracity of this assumption in a closely related system.[1] In the strictest sense, the heats of formation derived by using this assumption are upper limits to the true values.

A check on the thermochemistry derived in this section is the derivation for both protiated and deuteriated species. These should yield the same values once differences in zero-point energies are included. The zero-point energy differences for the relevant species are listed in Table III as are the differences in heats of formation at 298 K.

There is some ambiguity in deriving this information which concerns the temperature of the species. Indeed, the thresholds measured here do not correspond precisely to any temperature since the experiment is clearly microcanonical. The assumption we use here is that, except for the kinetic energy of the reactant Si^+, all reactants and products are characterized by 298 K, the nominal temperature of the reactant silane. Conversion between values at 0 and 298 K is achieved by using the information in Table III. The ion heats of formation are calculated by using the convention that the electron is a monatomic gas. Values in Table I from literature references which use the "stationary electron" convention have been increased by 1.48 kcal/mol at 298 K.

SiH^+ (SiD^+). The heat of formation of this species at 0 K, 272.0 ± 1.2 kcal/mol, is rather reliably known from spectroscopic studies[6] and from earlier work in our laboratory (which gives 271.7 ± 1.4 kcal/mol).[1] The heat of formation at 298 K is 273.8 ± 1.2 kcal/mol, 1.8 kcal/mol higher, Table III. $\Delta H_f°(SiD^+)$ differs from this by less than 0.1 kcal/mol.

SiH (SiD). Several conflicting spectroscopic studies exist for this diatom. Douglas[30] reports $D°_0(SiH) = 3.191 \pm 0.25$ eV, while Verma[31] gives an upper limit of 3.06 eV. The JANAF tables[32] use Verma's upper limit in combination with analyses of Hildenbrand[33] and Rao and Lakshman[34] and recommend 2.98 ± 0.09 eV. The most recent experimental measurement is the spectroscopic work of Carlson et al.,[35] who interpret the spectrum to find 3.341 ± 0.025 eV. These bond energies, when combined with $\Delta H_f°_0(Si) = 106.66 \pm 1$ kcal/mol and $\Delta H_f°_0(H) = 51.634$ kcal/mol,[32] provide the heats of formation for SiH, 84.7 ± 5.8, ≥87.7, 89.6 ± 2, and 81.3 ± 1.2 kcal/mol, respectively. We have measured this value in reaction 43, endothermic by 3.22 ± 0.04

$$Si^+ + CH_4 \rightarrow SiH + CH_3^+ \quad (43)$$

eV. When $\Delta H_f°(CH_3^+)$ is taken as 263.5 ± 1 kcal/mol,[36] this gives $\Delta H_f°(SiH) = 90.0 \pm 1.7$ and, at 0 K, 89.6 ± 1.7 kcal/mol. This is in excellent agreement with the value adopted by JANAF and clearly discounts Carlson et al.'s analysis.

SiH_2^+ (SiD_2^+). This species is formed in reactions 17 (19) and 21 (23); however, to obtain $\Delta H_f°(SiH_2^+)$ from the endothermicity of these reactions, $\Delta H_f°(SiH_2)$ must be known. Instead, we have chosen to measure $\Delta H_f°(SiH_2^+)$ independently and then determine $\Delta H_f°(SiH_2)$, see below. Reactions 44–46 are used for this purpose

$$Si^+ + C_2H_6 \rightarrow SiH_2^+ + C_2H_4 \quad (44)$$

$$Si^+ + C_3H_8 \rightarrow SiH_2^+ + C_3H_6 \quad (45)$$

$$Si^+ + C_2H_4 \rightarrow SiH_2^+ + C_2H_2 \quad (46)$$

and are analyzed as indicated in Table II. These yield $\Delta H_f°(SiH_2^+) = 274.3 \pm 1.4$, 277.5 ± 1.4, and 274.9 ± 1.4 kcal/mol. Consistent with these values are the results from reaction 47, Table

$$Si^+ + C_2D_6 \rightarrow SiD_2^+ + C_2D_4 \quad (47)$$

II, which yields $\Delta H_f°(SiD_2^+) = 277.4 \pm 1.4$ kcal/mol. When corrected for the difference in zero-point energies, Table III, this gives $\Delta H_f°(SiH_2^+) = 277.6 \pm 1.4$ kcal/mol. These four values when averaged give 276.1 ± 1.7 kcal/mol.

This value agrees with most recent photoionization (PI) work, Table I, 278.8,[2] 279.2,[37] and 277.7[38] kcal/mol, but clearly deviates from the value of Börlin et al.,[3] 264.5 kcal/mol. The average value of our work and the first three PI values are 278.0 ± 1.4 kcal/mol. This is taken to be the most definitive value.

SiH_2 (SiD_2). This product is formed in the highest energy process among the reactions involving Si–Si bond cleavage of the $Si_2H_4^+$ intermediate. For this reason it may be more susceptible to having a slow onset than other reaction processes. As noted above, this means that the value derived is most strictly viewed as an upper limit. Combining the endothermicity of reaction 17, Table II, with $\Delta H_f°(SiH_2^+) = 276.1 \pm 1.7$ kcal/mol yields $\Delta H_f°(SiH_2) = 68.9 \pm 2.3$ kcal/mol. From analysis of reaction 19, we find $\Delta H_f°(SiD_2) = 70.6 \pm 2.3$ kcal/mol which, when corrected for zero-point energy effects, gives $\Delta H_f°(SiH_2) = 70.7 \pm 2.3$ kcal/mol. An additional value of 67.4 ± 2.7 kcal/mol comes from analysis of reaction 48. These three values average to 69.0

$$^{28}SiH^+ + SiH_4 \rightarrow {}^{28}SiH_3^+ + SiH_2 \quad (48)$$

(29) Talrose, V. L.; Vinogradov, P. S.; Larin, I. K. *Gas Phase Ion Chemistry*; Bowers, M. T., Ed.; Academic: New York, 1979; p 305.
(30) Douglas, A. E. *Can. J. Phys.* **1957**, *35*, 71.
(31) Verma, R. D. *Can. J. Phys.* **1965**, *43*, 2136.
(32) JANAF Thermochemical Tables, Dow Chemical Company, distributed by Clearinghouse for Federal Scientific and Technical Information, PB168370 (1965) and subsequent updates.
(33) Hildenbrand, D. L., as cited in ref 32.
(34) Rao, T. V. R.; Lakshman, S. V. J. *Physica* **1971**, *56*, 322.
(35) Carlson, T. A.; Duric, N.; Erman, P.; Larsson, M. *J. Phys. B* **1978**, *11*, 3667.
(36) This heat of formation uses $\Delta H_f°(CH_3) = 35.1 \pm 0.2$ kcal/mol [McMillen, D. F.; Golden, D. M. *Annu. Rev. Phys. Chem.* **1982**, *33*, 493] and $IP(CH_3) = 9.84 \pm 0.02$ eV [Houle, F. A.; Beauchamp, J. L. *J. Am. Chem. Soc.* **1979**, *101*, 4067].
(37) Corderman, R. R.; Beauchamp, J. L., unpublished results. These authors are quoted in ref 42 for $\Delta H_f°(SiH_2^+) = 277.7 \pm 0.7$ kcal/mol and an appearance potential for SiH_3^+ from SiH_4 or 12.10 ± 0.05 eV which leads to $\Delta H_f°(SiH_3^+) = 235.1 \pm 1.3$ kcal/mol. Both values use the stationary electron convention.
(38) Berkowitz, J.; Greene, J. P.; Cho, H.; Ruscic, B. *J. Chem. Phys.* **1987**, *86*, 1235. All values in this paper are at 0 K. Citations here have been corrected to 298 K by using Table III.

Table IV. Ionization Potentials (eV) for Silicon Species

species	this work	literature exptl	literature theory
Si		8.152[a]	
SiH	7.89 (0.07)	7.91 (0.01)[b]	7.81,[c] 7.93
SiH_2	8.92 (0.07)	9.02 (0.02) or 9.15 (0.02)[b]	9.18[c]
SiH_3	8.11 (0.07)	8.01 (0.02),[b] 8.14 (0.01)[e]	7.99[c]
Si_2	≤8.04 (0.13)	7.4 (0.3),[f] 7.3[f]	7.61,[g] 7.5[h]
Si_2H	≤6.89 (0.13)[i]		
Si_2H_2	≤7.68 (0.16)[i]		
Si_2H_3	6.88 (0.14)[i]		

[a] Reference 13. [b] Reference 38. [c] Reference 43. [d] Rosmus, P.; Meyer, W. *J. Chem. Phys.* **1977**, *66*, 13. [e] Reference 42. [f] Reference 47. [g] Bruna, P. S.; Hirsh, G.; Buenker, R. J.; Peyerimhoff, S. D. *Molecular Ions*; Berkowitz, J., Groeneveld, K., Eds.; Plenum: New York, 1983; p 309. [h] Reference 46. [i] Derived by using neutral heats of formation from ref 9 and our measured ionic heats of formation.

± 2 kcal/mol. Note that this value utilizes only information obtained in the present experiments. If we use $\Delta H_f°(SiH_2^+)$ = 278.0 ± 1.4 kcal/mol as recommended above, the results of reactions 17 and 19 yield an average value for $\Delta H_f°(SiH_2)$ of 67.9 ± 2 kcal/mol.

Either of the values derived above is in accord with the recent ICR result of $\Delta H_f°(SiH_2)$ = 69 ± 3 kcal/mol recommended by Shin et al.,[5] the ab initio calculation, 68.1 kcal/mol, by Ho et al.,[8] and the recommendation of Jasinski.[4] It disagrees with the commonly accepted value of 58 kcal/mol recommended by Walsh[39] and with the ab initio calculation of 63.4 kcal/mol by Pople et al.[7] Walsh has recently reviewed the early kinetic work and presently recommends a value of 65.3 ± 1.5 kcal/mol.[40] Most recently Berkowitz et al.[38] derive a value of 65.2 ± 0.7 or 68.2 ± 0.8 kcal/mol. The ambiguity results from two possible values for the ionization potential of SiH_2. This is discussed further below. Our results favor the larger of these two values.

SiH_3^+ (SiD_3^+). Given the heat of formation of SiH determined above, the endothermicity of reaction 22 yields $\Delta H_f°(SiH_3^+)$ = 236.3 ± 2.3 kcal/mol. In the SiD_4 system, reaction 24 yields $\Delta H_f°(SiD_3^+)$ = 236.8 ± 2.3 kcal/mol, which gives $\Delta H_f°(SiH_3^+)$ = 237.8 ± 2.3 kcal/mol. The average value of 237.1 ± 2 kcal/mol is close to the four photoionization values listed in Table I, which average to 237.7 ± 1.3 kcal/mol, and to the ab initio result of 233 kcal/mol. The average value of our work and the four PI values is 237.5 ± 1.2 kcal/mol. We take this to be the definitive value.

SiH_3 (SiD_3). The neutral product accompanying formation of SiH^+ in reaction 6 is SiH_3. Combining the measured endothermicity of reaction 6 with $\Delta H_f°(SiH^+)$ = 273.8 ± 1.2 kcal/mol yields $\Delta H_f°(SiH_3)$ = 48.6 ± 2 kcal/mol. Similarly, reactions 11 and 13 provide $\Delta H_f°(SiD_3)$ = 47.4 ± 2 and 47.7 ± 2 kcal/mol. The difference in the heats of formation of SiH_3 and SiD_3 should be 0.9 kcal/mol, Table III, such that these latter values yield 48.3 ± 2 and 48.6 ± 2 kcal/mol for $\Delta H_f°(SiH_3)$. The average of these three values yields $\Delta H_f°(SiH_3)$ = 48.5 ± 1.6 kcal/mol. This is somewhat higher than the value determined by Doncaster and Walsh, 46.4 ± 1.2 kcal/mol,[39,41] but is within the combined uncertainties. Theoretical values, Table I, lie between these experimental determinations. Some support for the larger value for $\Delta H_f°(SiH_3)$ comes from the ionization potential (IP) measurements of Dyke et al.[42] and Berkowitz et al.,[38] Table IV. When these IPs are combined with $\Delta H_f°(SiH_3^+)$ = 237.5 ± 1.2 kcal/mol, $\Delta H_f°(SiH_3)$ is found to equal 48.3 ± 1.2 and 51.3 ± 1.3 kcal/mol, respectively.

Ionization Potentials of SiH_n. From the heats of formation of SiH_n and SiH_n^+ determined above, the adiabatic ionization potentials (IP) listed in Table IV can be determined by using eq 49.

$$IP(SiH_n) = \Delta H_f°(SiH_n^+) - \Delta H_f°(SiH_n) - 1.48 \text{ kcal/mol} \quad (49)$$

The final term corrects for the heat capacity of the electron at 298 K ($^5/_2RT$). The value for IP(SiH) derived from our results, Table IV, is in very good agreement with the direct determination by Berkowitz et al.[38] and can be compared favorably with the theoretical values as well. The IP of SiH derived by using the heats of formation for SiH and SiH^+ recommended above is 7.91 eV.

From the heats of formation of SiH_2^+ (276.1 kcal/mol) and SiH_2 (69.0 kcal/mol) derived in our studies, a value for IP(SiH_2) of 8.92 ± 0.07 eV is obtained. This value strongly supports the lower of the two directly measured IP values, 9.02 ± 0.02 or 9.15 ± 0.02 eV.[38] A theoretical value of 9.18 kcal/mol is high largely because the calculated value for $\Delta H_f°(SiH_2)$ is low, 63.4 kcal/mol.[43] If the directly measured IP of 9.02 ± 0.02 eV is combined with the recommended value of $\Delta H_f°(SiH_2^+)$ = 278.0 kcal/mol, $\Delta H_f°(SiH_2)$ is derived as 68.5 ± 1.5 kcal/mol. This value is recommended here and provides a consistent set of thermochemistry for SiH_2 and SiH_2^+.

The value of IP(SiH_3) obtained here, 8.11 ± 0.07 eV, cannot unambiguously differentiate between the photoionization values of Dyke et al., 8.14 ± 0.01 eV,[42] and Berkowitz et al., 8.01 ± 0.02 eV.[38] The disagreement between these experimental values is close to the vibrational spacing observed in these spectra, 0.102 ± 0.005[42] and 0.104 eV,[38] but could also be due to hot bands. The theoretical value of 7.99 eV[43] tends to support the lower value. As noted above however, if $\Delta H_f°(SiH_3^+)$ is taken to be 237.5 ± 1.2 kcal/mol as determined above, then the higher IP implies $\Delta H_f°(SiH_3)$ = 48.3 kcal/mol while the lower IP implies $\Delta H_f°(SiH_3)$ = 51.3 kcal/mol. A comparison with Walsh's value and the theoretical values, Table I, tends to favor the higher IP value.

It is interesting to obtain a substantially higher adiabatic ionization potential for SiH_2, 9.02 eV, than those of SiH_n (n = 0, 1, 3), Table IV. Si, SiH, $SiH_2(^3B_1)$, and SiH_3 all have one or more electrons in singly occupied non-bonding orbitals with extensive p character. It therefore seems reasonable that these species should have similar ionization potentials. This has recently been verified by Berkowitz et al. who measure IP[$SiH_2(^3B_1)$] = 8.24 ± 0.03 eV.[38] The difference between this value and the ionization potential of the $SiH_2(^1A_1)$ ground state is the singlet–triplet splitting. From our value for the IP of 8.92 eV, the splitting is 0.68 ± 0.08 eV, in agreement with values calculated by Schaefer and co-workers, 0.73 eV,[44] and by Luke et al., 0.74 eV.[23] Berkowitz et al. find that the singlet–triplet splitting is either 0.78 or 0.91 ± 0.03 eV. Our results and the theoretical values clearly support the lower of these, which corresponds to IP(SiH_2) = 9.02 eV. One further piece of experimental information is an upper limit on the singlet–triplet splitting of 0.6 eV determined by Lineberger and co-workers.[45]

Si_2^+. Si_2^+ is formed in reactions 25 and 26, which require the ejection of two hydrogen molecules. Consequently, the measured threshold for this process is more likely to be an upper limit than for other processes. Analysis of reaction 25 yields $\Delta H_f°(Si_2^+)$ ≤ 328.6 ± 2 kcal/mol while reaction 26 gives ≤327.3 ± 2 kcal/mol such that the average is ≤328.0 ± 2 kcal/mol. This yields a bond energy, $D°(Si^+–Si)$, of ≥76.8 ± 2.5 kcal/mol. A recent theoretical value for this binding energy is 88 kcal/mol.[46] From $\Delta H_f°(Si_2)$ = 141 ± 3 kcal/mol,[32] the ionization potential of Si_2 can be calculated as ≤8.04 ± 0.13 eV. This is substantially higher than the values, 7.4 ± 0.3 and 7.3 eV,[47] obtained by electron impact

(39) Walsh, R. *Acc. Chem. Res.* **1981**, *14*, 246.
(40) Frey, H. M.; Walsh, R.; Watts, I. M. *J. Chem. Soc., Chem. Commun.* **1986**, 1189.
(41) Doncaster, A. M.; Walsh, R. *J. Chem. Soc., Chem. Commun.* **1979**, 904; *Int. J. Chem. Kinet.* **1981**, *13*, 503.
(42) Dyke, J. M.; Jonathan, N.; Morris, A.; Ridha, A.; Winter, M. J. *Chem. Phys.* **1983**, *81*, 481.
(43) Pople, J. A.; Curtiss, L. A. *J. Phys. Chem.* **1987**, *91*, 155.
(44) Colvin, M. E.; Grev, R. S.; Schaefer, H. F., III; Bicerano, J. *Chem. Phys. Lett.* **1983**, *99*, 399. Meadows, J. H.; Schaefer, H. F., III. *J. Am. Chem. Soc.* **1976**, *98*, 4383.
(45) Kasdan, A.; Herbst, E.; Lineberger, W. C. *J. Chem. Phys.* **1975**, *62*, 541.
(46) Raghavachari, K.; Logovinsky, V. *Phys. Rev. Lett.* **1985**, *55*, 2853.
(47) Drowart, J.; Maria, G. D.; Inghram, M. G. *J. Chem. Phys.* **1958**, *29*, 1015. Verhaegen, G.; Stafford, F. E.; Drowart, J. *J. Chem. Phys.* **1964**, *40*, 1622.

with high-temperature mass spectrometry. These lower values may be inaccurate due to the effect of hot bands on the measurement of $IP(Si_2)$.

Si_2H^+ (Si_2D^+). The endothermicity of reaction 29, Table II, yields $\Delta H_f°(Si_2H^+)$ = 305.3 ± 2 kcal/mol. Reaction 31 gives a similar value for $\Delta H_f°(Si_2D^+)$ of 303.6 ± 2 kcal/mol. We assume the difference in heats of formation of the protiated and deuteriated species is negligible. A third independent value of 304.4 ± 2 kcal/mol is obtained from analysis of reaction 50, Table

$$^{28}SiH^+ + SiH_4 \rightarrow {}^{28}Si_2H^+ + 2H_2 \quad (50)$$

II. The average of these three values yields a best value for $\Delta H_f°(Si_2H^+)$ of 304.4 ± 1.6 kcal/mol. Because of the competition with other $Si_2H_n^+$ products, this is probably best viewed as an upper limit. The only literature values available for comparison come from electron-impact ionization measurements of Si_2H_6.[48,49] However, the earlier work of Potzinger and Lampe[48] is flawed by the isotope overlap problem discussed above. The more recent measurements of Chatham et al.[49] are included in Table I.

$Si_2H_2^+$ ($Si_2D_2^+$). The fact that formation of this product in reaction 32 (33) is exothermic gives an upper limit to $\Delta H_f°(Si_2H_2^+)$ of 305.3 ± 1.1 kcal/mol (303.8 ± 1.1 for $Si_2D_2^+$). A value of ≤268.0 ± 2.6 kcal/mol is obtained from analysis of reaction 51, Table II. This value now gives the exothermicity

$$SiH^+ + SiH_4 \rightarrow Si_2H_2^+ + H_2 + H \quad (51)$$

of reaction 32 as 1.62 ± 0.12 eV. This heat of formation is lower than the value obtained by electron-impact ionization, Table I.[49] By use of our value and the heat of formation of Si_2H_2 calculated by Ho et al.,[9] $IP(Si_2H_2)$ is found to be ≤7.68 ± 0.16 eV.

$Si_2H_3^+$ ($Si_2D_3^+$). From the endothermicity of reaction 36 (38), Table II, comes $\Delta H_f°(Si_2H_3^+)$ = 266.3 ± 2 kcal/mol (264.9 ± 1.5 for $Si_2D_3^+$). This does not agree very well with the value from electron-impact ionization,[49] Table I, although this has a very large error. The IP of Si_2H_3 calculated by using this value and the calculated neutral heat of formation is given in Table IV.

Acknowledgment. This work was supported by the National Science Foundation (Grant No. CHE-8608847). B.H.B. is grateful to J. L. Elkind, N. Aristov, and K. M. Ervin for their help in conducting these experiments. We would like to thank Drs. R. Walsh, J. Berkowitz, and L. A. Curtiss for providing their papers before publication.

Registry No. Si^+, 14067-07-3; SiH_4, 7803-62-5; $Si_2H_2^+$, 39373-18-7; SiH, 13774-94-2; SiH_2, 13825-90-6; SiH_3, 13765-44-1; SiH_2^+, 28149-31-7; SiH_3^+, 41753-67-7; Si_2^+, 12597-36-3; Si_2H^+, 39373-15-4; $Si_2H_3^+$, 39373-99-4; Si_2, 12597-35-2; Si_2H, 102437-78-5; Si_2H_2, 36835-58-2; Si_2H_3, 12135-45-4.

(48) Potzinger, P.; Lampe, F. W. *J. Phys. Chem.* **1969**, *73*, 3912.
(49) Chatham, H.; Hils, D.; Robertson, R.; Gallagher, A. *J. Chem. Phys.* **1984**, *81*, 1770.

Spontaneously Organized Molecular Assemblies. 4. Structural Characterization of *n*-Alkyl Thiol Monolayers on Gold by Optical Ellipsometry, Infrared Spectroscopy, and Electrochemistry

Marc D. Porter,*§† Thomas B. Bright,† David L. Allara,*† and Christopher E. D. Chidsey‡

Contribution from Bell Communications Research, Red Bank, New Jersey 07701, and AT&T Bell Laboratories, Murray Hill, New Jersey 07974. *Received September 22, 1986*

Abstract: Monolayer assemblies on *n*-alkyl thiols $(CH_3(CH_2)_nSH$ where n = 1, 3, 5, 7, 9, 11, 15, 17, and 21), adsorbed on gold from dilute solution, have been characterized by optical ellipsometry, infrared (IR) spectroscopy, and electrochemistry. All three techniques show that there are distinct differences in structure between long- and short-chain thiol monolayers. The value of n for the sharpest change varies between 5 and 11 depending upon the specific measurement. The IR spectroscopic and ellipsometric data indicate that the long-chain thiols form a densely packed, crystalline-like assembly with fully extended alkyl chains tilted from the surface normal by 20–30°. As the chain length decreases, the structure becomes increasingly disordered with lower packing density and coverage. Electrochemical measurements of heterogeneous electron-transfer rates and of differential capacitance indicate that the long-chain monolayers are free of measurable pin holes, provide substantial barriers to electron transfer, and are strongly resistant to ion penetration. In contrast, with decreasing chain length the barrier properties become weaker. Taken together, these results demonstrate that monolayer assemblies of long-chain thiols on gold have significant potential as model systems for studies of heterogeneous electron transfer, ion transport, and double-layer phenomena.

The organization of monomolecular assemblies at solid surfaces provides a rational approach for fabricating interfaces with a well-defined composition, structure, and thickness. Such assemblies could provide a means to control the chemical and physical properties of interfaces for a variety of heterogeneous phenomena including catalysis,[1-3] corrosion,[4] lubrication,[5,6] and adhesion.[7] The ability to control interfacial processes has important implications from the point of view of both fundamental and technological advances. For example, pin-hole-free, ionically insulating molecular films of monolayer thickness with well-defined structure

§ Present address: Department of Chemistry, Iowa State University, Ames, Iowa 50011.
† Bell Communications Research.
‡ AT&T Bell Laboratories.

(1) Somorjai, G. A. *Chemistry in Two Dimensions: Surfaces*; Cornell University Press: Ithaca, NY, 1981.
(2) Murray, R. W. In *Electroanalytical Chemistry*; Bard, A. J., Ed.; Marcel Dekker: New York, 1984; Vol. 13.
(3) Durand, R. R.; Bencosme, C. S.; Collman, J. P.; Anson, F. C. *J. Am. Chem. Soc.* **1983**, *105*, 2710–2718.
(4) Notoya, T.; Poling, G. W. *Corrosion* **1979**, *35*, 193–200.
(5) Zisman, W. A. In *Friction and Wear*; Davies, R., Ed.; Elsevier: New York, 1959.
(6) Bowden, F. P.; Tabor, D. *The Friction and Lubrication of Solids*; Oxford University Press: London, 1968.

0002-7863/87/1509-3559$01.50/0